Aerodynamic and Aeroacoustic
Three-Dimensional Design for a "Silent" Aircraft

J.I. Hileman,[*] Z.S. Spakovszky,[†] M. Drela [‡]
Gas Turbine Laboratory, Department of Aeronautics and Astronautics,
Massachusetts Institute of Technology, Cambridge, MA 02139

and

M.A. Sargeant[§]
Cambridge University Engineering Department,
Trumpington Street, Cambridge CB2 1PZ, UK

This paper presents a three-dimensional airframe design methodology for low noise emission and high fuel efficiency, based on a blended-wing-body type aircraft. The design methodology uses a combination of high and low fidelity tools to assess the performance and acoustics of the aircraft. The goal set by the Silent[**] Aircraft Initiative is a viable, commercial aircraft design with noise levels imperceptible outside the airport perimeter in a well-populated urban environment. To be viable, the aircraft requires a fuel burn comparable to modern conventional aircraft. The detailed airframe design incorporates leading edge camber of the centerbody to provide pitch trim without penalties in induced drag, wave drag, and trim drag. A low noise approach is achieved with reduced approach velocity and increased distance between the airframe and the observer. This slow and steep approach profile is enabled through a combination of thrust vectoring, quiet drag generation, and leading edge high-lift devices. The blended-wing-body type airframe design presented in this paper is both quiet with an OASPL of approximately 65 dBA and highly efficient with a cruise ML/D of 18.5. The paper concludes with ideas to further reduce noise to meet the aggressive SAI goal with minimal cruise performance penalty.

Nomenclature

b	=	span
c	=	chord
C_D	=	drag coefficient
C_f	=	skin friction coefficient
C_L	=	lift coefficient
C_m	=	moment coefficient
D_p	=	pressure drag
D_f	=	friction drag
D_R	=	$\dot{m}u$, ram drag
d/l	=	ratio of diameter-to-length for equivalent body of revolution
L/D	=	lift-to-drag ratio
$\dot{m}$	=	mass flow through the engines

---

[*] Post-Doctoral Associate, hileman@mit.edu, AIAA Member.
[†] Associate Professor, AIAA Member.
[‡] Professor, AIAA Member.
[§] Ph.D. Student, AIAA Member.

[**] "Silent" in the context of this research does not refer to the absence of acoustic sources; instead, it is meant to reflect the step change in noise reduction.
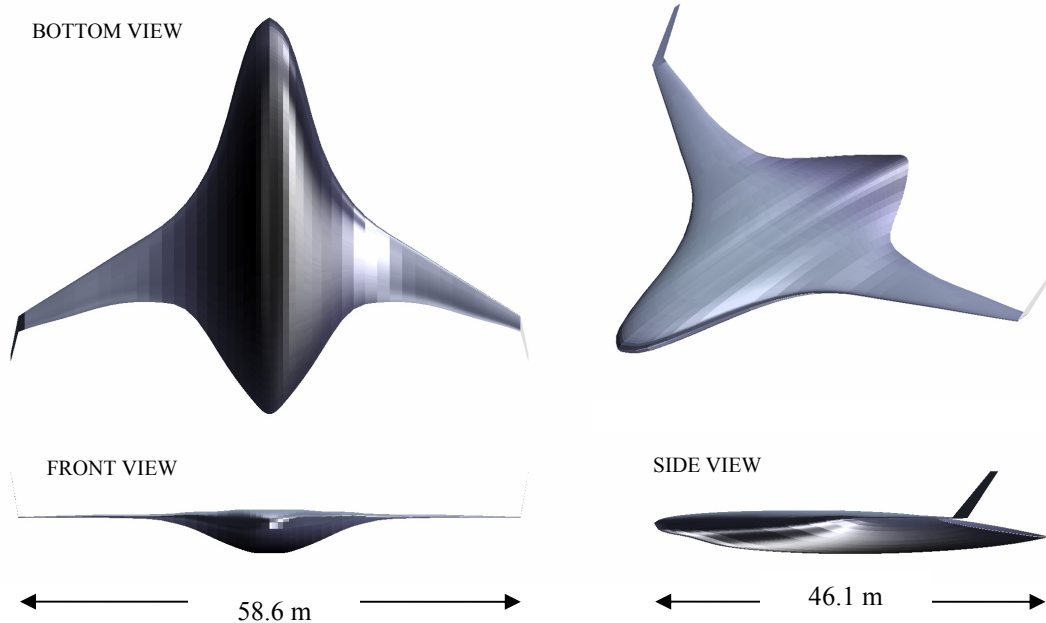
BOTTOM VIEW

FRONT VIEW

SIDE VIEW

58.6 m

46.1 m

Figure 1. Three-dimensional view of the current Silent Aircraft eXperimental airframe design.

M	=	Mach number
OASPL	=	overall sound pressure level, dBA
r	=	distance from noise source to observer
Re	=	Reynolds number based on length
S	=	aircraft trapezoidal area
SPL	=	sound pressure level, dB
t/c	=	airfoil thickness to chord ratio
u	=	aircraft velocity
u_{jet}	=	jet exit velocity
W	=	aircraft weight
α	=	aircraft angle of attack
β	=	thrust vector angle
ΔC_D	=	drag augmentation provided by quiet drag devices
δ_t	=	outer-wing twist, degrees
ρ	=	density
η	=	normalized spanwise coordinate
Λ	=	mid-chord sweep

I.   Introduction

The Silent Aircraft Initiative (SAI), a collaborative effort between the Massachusetts Institute of Technology and the University of Cambridge funded by the Cambridge-MIT Institute, aims to design an aircraft inaudible outside the airport boundary within a well populated, urban environment. To achieve this step change in noise reduction, noise has to become a primary variable in the aircraft design process.[1] The outcome of this research effort is a credible Silent Aircraft eXperimental design (SAX), which not only aims to meet ambitious levels of noise reduction, but achieves a fuel burn competitive to the current generation of aircraft (e.g., Boeing 787). The current SAX design, shown in Figure 1, is a blended-wing-body type airframe with three embedded, boundary layer ingesting core engines that drive nine fans. The aircraft is designed to carry 215 passengers in a three-class configuration a distance of 5,000 nm. This paper presents the detailed three-dimensional aerodynamic and aeroacoustic design of this aircraft.
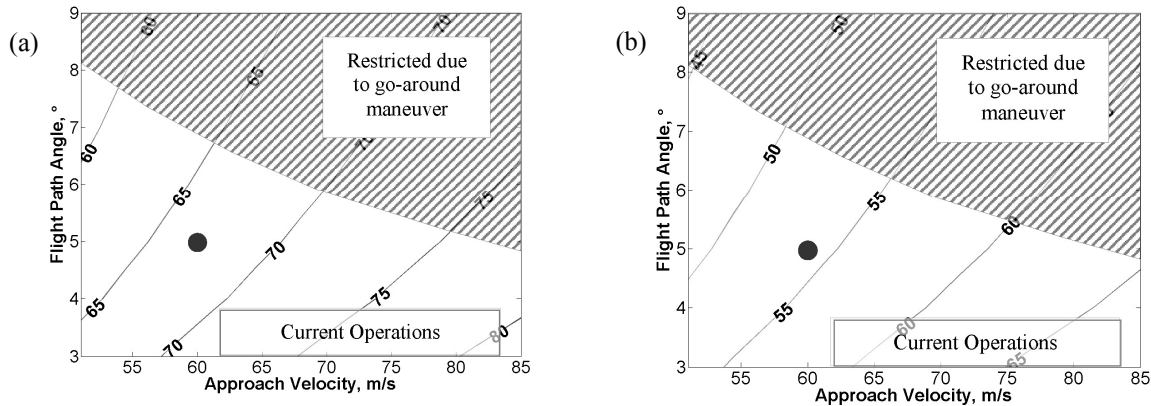
Figure 2. Undercarriage (a) and airfoil (b) OASPL (dBA) for various approach profiles of the SAX aircraft. Range of current aircraft operations are marked by a box. Approach profiles that are restricted due to the need for a go around maneuver are marked by the hatched region. A desired approach profile is marked by the dot.

A. Nature of the Problem

During take-off, the reduction of jet noise is the primary challenge. The SAI noise goal can be achieved while achieving low specific fuel consumption by combining a very high bypass ratio engine cycle with a variable area nozzle.[2,3] The forward radiated fan noise can be shielded by the planform[4] and a careful design of the engine for low noise emission[5] suggests that the noise goal is achievable on take-off.[6]

During approach, airframe noise is dominant with source contributions from the undercarriage, the high-lift devices, the control surfaces, drag augmentation, and the scattering of boundary layer turbulence at the trailing edges commonly referred to as airfoil self-noise. The sound pressure level from these noise sources have an intensity proportional to $1/r^2$ and u^n where n is 5 for trailing edge scattering and 6 for dipole type sources such as the undercarriage. The scaling law thus suggests that the noise at the observer location can be reduced by using steep and slow approach profiles. The aerodynamic design required for such a quiet landing is the focus of this paper.

The loudest component of the airframe is the undercarriage. Estimates of the approach noise emitted by the undercarriage as well as that from airfoil self-noise of the SAX aircraft are shown in Figure 2 for various approach profiles. Current aircraft operations are marked by a box. Airfoil self-noise is the quietest noise source and provides an estimate of the minimum airframe noise level if all other sources were eliminated. Combinations of velocity and flight path angle that are restricted and limited by the need for a go around maneuver (discussed later) are highlighted by the hatched region in Figure 2. Slat noise was found to be quieter than the undercarriage and is not shown here.[6] The ground noise estimates were computed using semi-empirical relationships[7-9] with an undercarriage comprised of two four-wheel main bogeys and a single dual-wheel nose bogey sized using correlations by Raymer.[10] By streamlining the wheels and struts of the undercarriage, Jaeger[11] was able to achieve a 13 dBA decrease in undercarriage noise emission on a 6 wheel landing gear unit. However, using undercarriage fairing alone with an approach within the current operating regime will not achieve the SAI goal. In addition to streamlining, the aircraft approach profile needs to be modified to reduce undercarriage noise. An approach trajectory with an approach speed of 60 m/s and a flight path angle of 5° combined with undercarriage noise reduction of 13 dBA through streamlining is suggested to meet the noise goal of the silent aircraft.

The challenge is to achieve a slow and steep approach profile with minimal impact on cruise performance. For noise reasons, the idea is to use minimum aircraft reconfiguration through deployable devices on approach. As shown by the sensitivity of undercarriage noise to approach profile, the aeroacoustic signature of the aircraft is directly related to the aerodynamic performance. Aerodynamic and acoustic design tools have to be combined to achieve the noise goal, and the tradeoff between cruise L/D and approach noise must be assessed to understand what penalty is paid. This paper presents a novel design methodology that unites three-dimensional aerodynamic design with aircraft operations and aeroacoustic considerations.

Blended-wing-body type aircraft have the advantage of low noise emission due to their lack of extraneous surfaces and simple trailing edges. Such airframe configurations enable the embedding of a highly integrated

American Institute of Aeronautics and Astronautics

propulsion system with significant engine noise shielding as shown in Figure 1. The lack of tail surfaces prevents the use of flaps on approach because there is no means of trimming the generated pitching moment. This paper introduces enabling technologies to overcome these challenges and establishes a framework for their aerodynamic and aeroacoustic assessment.

To achieve a fuel burn comparable to modern aircraft, the Breguet range equation indicates that the Silent Aircraft will need to have engines with low specific fuel consumption, an efficient airframe design with a high ML/D (cruise Mach number times lift-to-drag ratio), and high structural efficiency (low empty weight to maximum take-off weight ratio).[12] The current
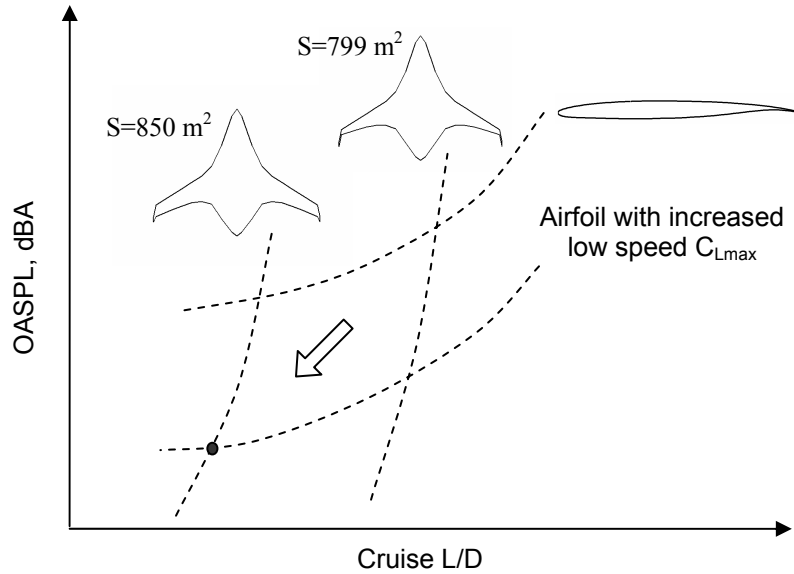

Figure 3. Hypothesized variation of noise emission and cruise performance with wing profile and area. The goal is to minimize the penalty in cruise L/D for a given decrease in OASPL.

silent aircraft engine design achieves a competitive SFC of 14.2 g/sN,[3] while the preliminary planform design by Diedrich et al.,[6] which forms the basis for this study, has a sufficiently high ML/D to overcome a relatively poor weight fraction to result in an aircraft with fuel burn better than a Boeing 787-3. To maintain this competitive fuel burn, the airframe for the silent aircraft needs to have an ML/D above 17.5 and empty weight fraction below 0.6.

The key question addressed by the ongoing work presented in this paper is what cruise performance penalties are generated for a low noise approach. This can be viewed in the context of Figure 3 where combinations of wing profile and planform area impact cruise L/D and approach noise levels. The goal is to achieve a low OASPL with minimal penalty in cruise L/D as indicated by the arrow. This paper presents a combination of technologies and a design philosophy to answer this question.

B. Conceptual Approach and Technical Roadmap
The ideas behind the design of an airframe with both low approach noise and competitive cruise performance are to:

- Increase centerbody leading edge camber for cruise pitch trim. The forward section of the centerbody airfoil is used to generate lift and to balance the pitching moment caused by the outer-wings at cruise conditions. The leading edge camber is adjusted to yield the desired airfoil twist and lift distribution with zero pitching moment at the beginning of cruise to minimize drag. Leading edge camber avoids canards and tail surfaces, and removes the necessity of reflex cambered airfoils; all of which detrimentally impact noise levels and airframe drag.

- Introduce thrust vectoring for pitch trim on approach. The noise reduction benefit of thrust vectoring compared to the edges and cavities of deflected control surfaces are twofold because the relatively low exhaust velocity and the alignment of the jet with the flight trajectory result in a reduction in turbulent mixing noise.

- Design the airframe for a slow approach trajectory using quiet, leading edge high-lift devices such as, for example, a drooped leading edge, leading edge suction, leading edge rotating cylinders, or slats with filled coves and gaps.

- Implement deployable quiet, high-drag devices for a steepened approach trajectory. The quiet drag augmentation will be provided by perforated spoilers to modify the wake turbulence for noise reduction[13] and engine air brakes.[14]

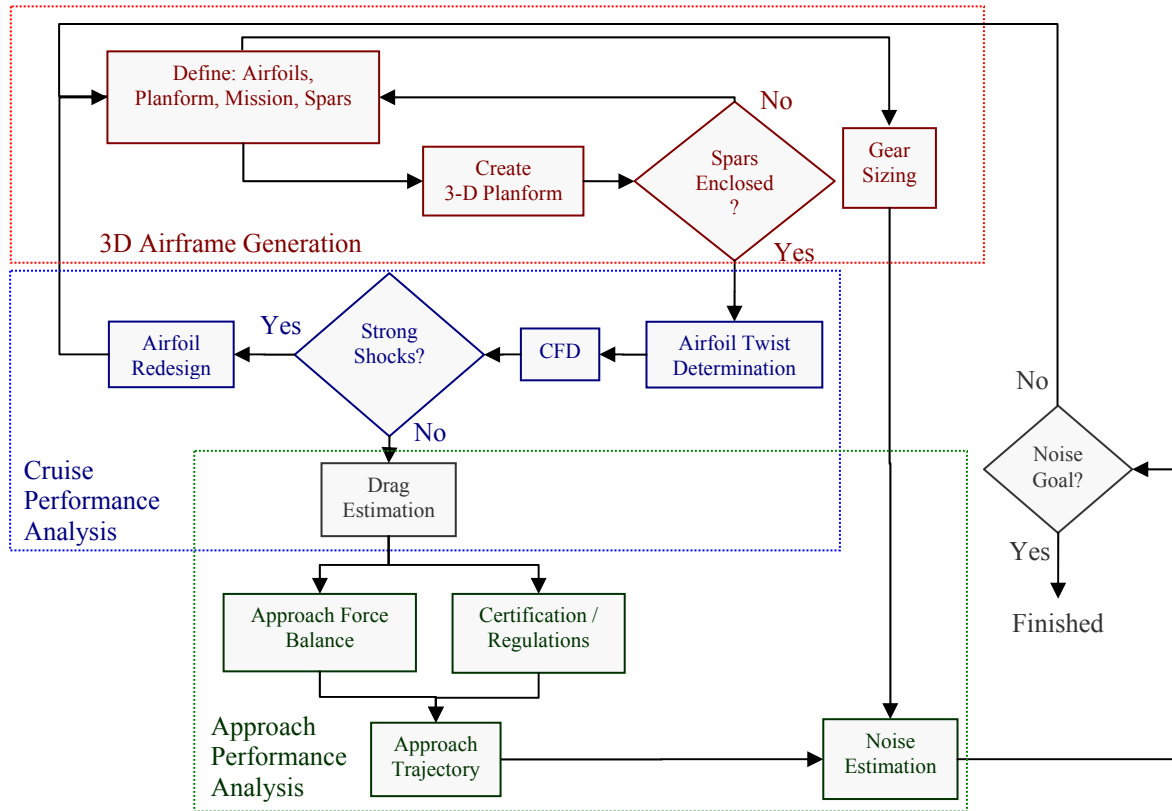- Fair the undercarriage for additional noise reduction, of up to 13 dBA.[11]

Figure 4. Schematic representation of the quasi-inverse, three-dimensional design process used to create the airframe in Figure 1. The framework is comprised of three main components: three-dimensional airframe generation, cruise performance analysis, and approach performance analysis.

Three-dimensional analysis needs to be employed because the airframe shape yields a highly three-dimensional aerodynamic design problem. As such, three-dimensional pressure relief on the centerbody leads to cross-flow on the junction between the centerbody and outer-wing and this can only be assessed by a three-dimensional calculation. However, three-dimensional viscous numerical simulations are not an appropriate option in the design phase where the design space needs to be explored and a short turn-around is required. To overcome this challenge, an effective, quasi-inverse, three-dimensional design methodology is established that combines vortex lattice methods with viscous, compressible two-dimensional airfoil analyses and three-dimensional inviscid, compressible numerical simulation. Pressure and friction drag coefficients are estimated using a combination of empirical correlations for bodies of revolution and the aforementioned two-dimensional airfoil analyses. This design methodology, shown schematically in Figure 4, can be broken up into three primary modules:

- **Three-dimensional airframe generation**. Sectional airfoil profiles are created from two-dimensional Bezier splines. These are combined with a two-dimensional planform defined by Diedrich et al.[6] to create the three-dimensional airframe. A check is made to ensure the airframe meets structural constraints.

- **Cruise aerodynamic assessment**. A vortex lattice method is used for trim analysis and determination of the airfoil twist distribution. Three-dimensional aspects of the centerbody are captured with an inviscid, compressible CFD solution for the entire airframe. A two-dimensional viscous, compressible airfoil analysis tool is used to analyze and redesign airfoil sections, if necessary. The drag from the airframe is estimated using the aforementioned tools with empirical correlations.

- **Approach aerodynamic and aeroacoustic assessment**. The high-lift, vectored thrust and drag requirements are estimated for a range of approach profiles with consideration of federal safety requirements. These are used with low speed two-dimensional airfoil analyses to yield the minimum approach velocity for the aircraft, which in turn yields the estimated airframe noise.

The establishment of each of these primary modules is the subject of this paper and is discussed in detail.

C. Scope of the Paper

The objectives of the ongoing work presented in this paper are to:

- Establish a high fidelity, quasi-inverse design methodology for the aerodynamic and aeroacoustic analysis of a quiet blended-wing-body type airframe (SAX).

- Define the detailed three-dimensional aerodynamic aircraft design for low approach noise levels and competitive cruise performance using the established design framework and enabling technologies such as for example thrust vectoring and leading edge camber.

- Quantify the necessary tradeoffs in cruise performance to achieve low approach noise levels and define limitations and technical barriers in the design space. Discuss the resulting design implications.
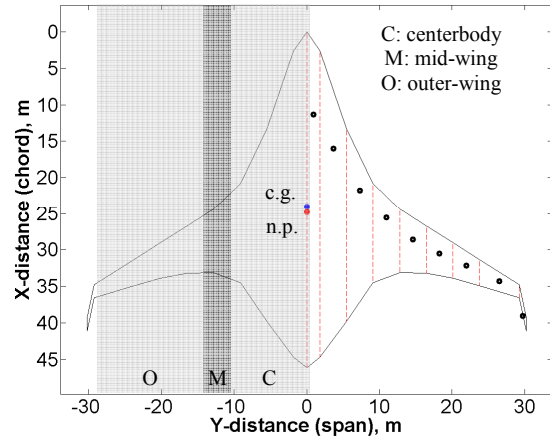

Figure 5. Sectional definition of airframe geometry. Black circles indicate airfoil sectional centers of pressure, the blue circle is the overall center of pressure and CG location, and the red circle is the neutral point of the aircraft.

II. Quasi-Inverse Three-Dimensional Design Methodology

The design methodology, shown schematically in Figure 4, combines high and low fidelity tools in a quasi-inverse and iterative manner. The process relies on three main components: three-dimensional airframe generation, cruise performance analysis, and approach performance analysis. The takeoff segment of the mission is currently being analyzed by the authors and is not discussed in this paper. The effects of vectored thrust and boundary layer ingestion on the airframe flow-field are not considered here, but are being addressed in other research.

A. Three-Dimensional Airframe Generation

The starting point for the generation of the three-dimensional airframe geometry is a modified version of a weight optimized planform by Diedrich et al.[6] which was created using Boeing's Multi-disciplinary Design Optimization code WingMOD.[15,16] The spar-box, weights, airfoil thicknesses and center of gravity as defined by WingMOD are used to define the structural constraints analyzed in this paper. The planform is divided into three sections that define the local airfoil profile as shown on the left hand side in Figure 5. The mid-wing region has an airfoil profile that is linearly interpolated between the centerbody and outer-wing. The airfoil suction and pressure surfaces are defined by two and three Bezier splines, respectively. The third Bezier spline shapes the profile and camber near the leading edge. Continuity of the profile slope is ensured at spline intersections. Each airfoil is scaled to yield the prescribed local thickness-to-chord ratio. The airfoil sections are lofted to create the three-dimensional airframe, which must enclose the rear spar, the front outer-wing spar, and the passenger cabin.

B. Cruise Performance Analysis

This section describes the aerodynamic design tools that are used to create an efficient airframe that is trimmed at the beginning of cruise without the need for deflected surfaces or thrust vectoring.

1. Determination of Airfoil Twist

The three-dimensional aircraft geometry is divided into nine spanwise sections as indicated by the dashed lines in Figure 5. This geometry is analyzed with AVL to determine the wing twist distribution that results in a zero net pitching moment at the beginning of cruise. AVL is a vortex lattice code with aerodynamic, trim, and stability analyses.[17] The twist distribution is defined by three linear segments: zero twist for $\eta < 0.06$, a linear increase to 95% of the maximum twist for $0.06 < \eta < 0.6$, and a linear increase to 100% of the maximum twist for $0.6 < \eta < 1$, where η is the normalized spanwise coordinate. Two geometries with different maximum wing twist are analyzed with AVL. The linear variation of C_L and C_m with angle of attack and outer-wing twist form two equations that can

be solved for the angle of attack and outer-wing twist required for $C_m = 0$ and $C_L = W/(\frac{1}{2}\rho u^2 S)$, where W is the maximum takeoff weight. This is mathematically expressed as

$$\begin{bmatrix} \dfrac{\partial C_L}{\partial \alpha} & \dfrac{\partial C_L}{\partial \delta_t} \\ \dfrac{\partial C_m}{\partial \alpha} & \dfrac{\partial C_m}{\partial \delta_t} \end{bmatrix} \begin{bmatrix} \Delta\alpha \\ \Delta\delta_t \end{bmatrix} = \begin{bmatrix} C_L - C_{L,\alpha_0} \\ C_m - C_{m,\delta_{t,0}} \end{bmatrix},$$ (1)

where the actual angle of attack and outer-wing twist are

$$\begin{aligned} \alpha &= \alpha_0 + \Delta\alpha \\ \delta_t &= \delta_{t,0} + \Delta\delta_t \end{aligned}.$$ (2)

The twist distribution and the geometry define the three-dimensional airframe, which is subsequently analyzed using three-dimensional numerical simulation.

2. Three-Dimensional Computational Fluid Dynamics

Next, the three-dimensional compressible flow around the airframe is calculated to capture the highly three-dimensional flow that develops over the centerbody. The main focus of this analysis is to locate possible shock waves and estimate their strength. This is important for both the drag from the airframe and integration of the propulsion system embedded in the airframe to ingest the boundary layers from the suction surface. Using Fluent, a three-dimensional inviscid Euler solution is constructed for the blended-wing-body type airframe defined in the previous steps. Given the large Reynolds numbers over the aircraft, an inviscid solution is deemed sufficient to capture the pressure distribution and to provide a guide to the shock location and strength. A three-dimensional, first-order upwind solution of the Euler equations is obtained using pressure far-field boundary conditions on an unstructured grid consisting of 1.1 million cells.

3. Two-Dimensional Airfoil Design

The three-dimensional inviscid flow solution is used iteratively with MSES v3.02, a two-dimensional compressible, viscous airfoil design and analysis tool,[18-20] with the aim to create an airframe without strong shocks. Two-dimensional airfoil profiles are manipulated and analyzed with MSES until the airframe is trimmed for pitch. The other constraint on the quasi-inverse two-dimensional design process is that the flow over the airfoil cannot exceed Mach 1.15 to ensure low wave drag. For the outer-wing profile design, the airfoil properties are modified by the mid-chord sweep angle, Λ, since the flow in this region is largely two-dimensional with fluid motion normal to the mid-chord line. The lift coefficient, Mach number, and local airfoil thickness are affected by the sweep angle according to $C_{L,swept} = C_L/\cos^2\Lambda$, $M_{swept} = M\cos\Lambda$, and $y_{swept} = y/\cos\Lambda$.[21] The flow over the centerbody is highly three-dimensional with considerable pressure relief so there is no obvious choice for a sweep angle. The initial centerbody design is thus conducted using an unswept profile through the center of the aircraft. This choice yields a conservative estimate of the Mach number due to the aforementioned pressure relief effect.

4. Drag Estimation

The total airframe drag cannot be determined using CFD since a viscous solution would be too time consuming and would result in unnecessary limits placed on the exploration of design space. Instead, the output from AVL and MSES are combined with empirical relations to yield the aircraft drag. The total drag on the aircraft is computed from the summation of the lift induced drag, pressure drag, skin friction drag, and wave (compressibility) drag from the centerbody, mid-wing, outer-wings, winglet and engine nacelles. The induced drag for the airframe is estimated using AVL. The drag bookkeeping does not take into account the drag reduction from boundary layer ingestion that results from embedding the propulsion system.

The pressure and friction drag from the centerbody are estimated using compressibility corrected, empirical relationships by Hoerner[21] for bodies of revolution measured at high Reynolds number. These data are based on Zeppelin measurements with Reynolds numbers approaching 10^{10}. The centerbody region, defined as $\eta < 0.44$, is converted to a body of revolution with equivalent surface area. The combined pressure and friction drag coefficients from such a body of revolution can be approximated by

$$C_{D,wet} = \left[\frac{0.03}{\mathrm{Re}^{1/7}} + \frac{0.0016}{\mathrm{Re}^{0.4}(d/l)} \right] \left[1 - 0.09M^2 \right] \left[1 + 1.15(d/l)^{1.5} + 6\left(1 - M^2\right)^{-0.6}(d/l)^3 \right],$$ (3)

where the diameter-to-length ratio (*d/l*) for the airframe is computed by dividing the equivalent diameter by the centerbody chord. The equivalent diameter is that required to have an area equivalent to the centerbody cross-section at its maximum thickness

$$d/l = \frac{1}{c_1}\sqrt{\frac{8b\langle c\rangle\langle t/c\rangle}{\pi}}\,,$$ (4)

where b and c_1 denote the centerbody span and chord, respectively. The expressions within the first bracketed term of Eqn. (3) are the skin friction coefficient for a three-dimensional body of revolution with a Reynolds number between 10^7 and 10^9. The second bracketed term corrects the skin friction coefficient for compressibility assuming a smooth surface. The third bracketed term, when multiplied by the skin friction coefficient, approximates the friction plus pressure drag coefficients of a conventional body of revolution, which is defined by a maximum diameter of 30 to 40% of the body length. The drag coefficient of Eqn. (3) is based on a wetted surface area of a streamlined body and is approximated by

$$S_{wet} = 3S_0\left(d/l\right)^{-1},$$ (5)

where S_0 is the surface area of the centerbody region.

The pressure and friction drag for the outer-wings are estimated using MSES on swept airfoil sections that had angle of attack adjusted to yield the sectional C_L for that airframe section. The pressure drag from the MSES analysis of the swept airfoil is converted to that of an unswept airfoil by $C_{Dp} = C_{Dp,swept}\cos^3\Lambda$.[21] At this stage of the design process, the winglets have not been adequately designed to yield an accurate drag estimate. As such, the pressure and friction drag from the outermost airfoil section are scaled based upon the area ratio to yield winglet friction and pressure drag.

The drag from the engine nacelles is computed using empirical relations by Shevell[22]

$$C_{D,nacelle} = KC_f\frac{S_{nacelle}}{S}\,,$$ (6)

where K=1.4 is a pressure drag correction factor and C_f is estimated from

$$0.242\big/\sqrt{C_f} = \log_{10}\left(C_f Re\right),$$ (7)

with Reynolds number based on nacelle length. The nacelle area, $S_{nacelle}$, is estimated using nine half-cylinders to crudely represent the embedded engine nacelles for a three core / nine fan design.

C. Approach Performance Analysis

The cruise performance analyses assess the airframe efficiency during cruise while the analyses presented in this section examine the performance of the airframe during final approach to landing. The approach performance consists in estimating the lift requirement, drag augmentation, and thrust vectoring needed to maintain a steady approach profile with consideration of the federal air safety requirements. The low speed aerodynamics of the airframe are then analyzed to determine the minimum approach velocity for the aircraft, which in turn yields the minimum noise for the airframe.

1. Approach Force Balance

Each approach profile, defined by an approach velocity and flight path angle, requires a unique combination of thrust vectoring, drag augmentation, and aircraft angle of attack to balance the aerodynamic forces and the aircraft weight. The force and moment balance together
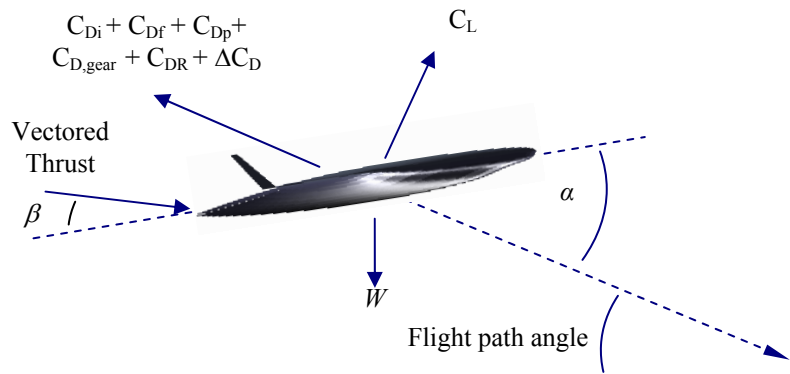

Figure 6. Aircraft force balance during a steady approach.

with the relation between engine ram drag and the vectored and net thrust of 32.8 kN are analyzed to determine the approach profile requirements. All of the forces acting on the aircraft are shown in Figure 6 where the drag terms are assumed to act through the center of gravity. The aerodynamic lift, computed using AVL, balances a component of the weight of the aircraft as well as a component of the vectored thrust. The aerodynamic pitching moment, also computed using AVL, balances the vectored thrust that acts on a moment arm of the centerbody length minus the location of the center of gravity. The drag balance is more complex since components of weight and vectored thrust are balanced by the total aircraft drag comprised of the aerodynamic drag, undercarriage drag, and ram drag as well as the drag created by drag augmentation devices. Depending on the approach profile, excess thrust or additional drag is required to keep the aircraft on a steady descent path (negative ΔC_D implies that added engine thrust is required). Undercarriage drag is determined using empirical relations by Raymer.[10] For any given approach profile, the force and moment balance equations are solved with the engine thrust relation to yield the angle of attack, α, thrust vectoring angle, β, and the quiet drag requirement, ΔC_D.

2. Certification / Regulation Considerations

According to the FAA, limitations on the approach trajectory include: (1) an approach speed above 1.23 times the stall speed (FAR 25.125), (2) the ability to land under auxiliary power, and (3) the performance of a go-around maneuver. The implications of the stall speed requirement on the airframe design are discussed in the next section. For the aircraft design considered in this paper, the auxiliary power landing is solved by using simple, hinged elevons located on the aft 25% chordwise extent of the airfoils located outboard of $\eta = 0.44$. These surfaces are also used for pitch and roll control.

Existing approach procedures with conventional aircraft utilize 3.0° to 3.4° flight path angles and a final approach speed between 60 m/s and 83 m/s as shown in Figure 2 (see Reynolds and Clarke[23] for a complete description). To fly beyond the range of the current operating regime, the Silent Aircraft needs to conduct a safe go-around procedure. A simplified model of the go-around scenario was created with the aircraft being modeled as a point mass moving on a circular arc. The model depends on three inputs: (1) decision height, the minimum height at which the pilot can abort the landing and start the go-around maneuver, (2) load limit factor, which is the passenger comfort limit for the aggressiveness of the maneuver measured in multiples of the gravitational acceleration, and (3) pilot/aircraft delay, the sum of time lags between the pilot's decision and the aircraft response including engine spool-up time. Currently, the most common minimum decision height is 100 ft. Experimental studies of pilot/aircraft delay times during final approach operations found typical values of 3-5 seconds.[24] Current operating guidelines for airline pilots suggest load factor limits of 1.3 g are appropriate for passenger comfort requirements.[25] The restricted, hatched area in Figure 2 is based on a decision height of 100 ft, pilot/aircraft delay of 3 seconds, and a load limit factor of 1.3g. The approach trajectory of 60 m/s and 5° flight path angle meets the above requirements.

3. Approach Trajectory

The approach force balance discussed in Figure 6 yields estimates of α, β, C_L, and ΔC_D regardless of their physical feasibility. To assess feasible approach trajectories, MSES is used to determine the low speed drag polar for the centerbody, mid-wing, and outer-wing airfoils. As discussed in the introduction, a variety of quiet leading edge high-lift devices are being assessed within the SAI research team for noise emission, maximum lift, and impact on drag. In the preliminary analysis reported here, the leading edge high-lift treatment is assumed to provide enough increased lift to offset the stall speed requirement. Thus, the minimum approach speed is determined by the maximum airfoil lift coefficient from the drag polar. Future work will improve this estimate. The noise due to the devices generating the additional drag required to keep the aircraft on the glide slope is assumed to be quieter than the undercarriage. Devices such as perforated spoilers[13] and engine air brakes[14] are currently being investigated for this purpose.

4. Noise Estimation

The noise emission from the slats and airfoils is estimated using empirical relationships by Fink,[7] and the undercarriage noise prediction is based on a method developed by Chinoy.[8] The empirical relationships depend on specific geometric details of the components in addition to global aircraft details such as approach velocity and altitude. The undercarriage noise estimate is mainly governed by wheel diameter and strut length for the nose and main gear, which are estimates from empirical sizing correlations by Raymer.[10] The nose gear strut length and diameter are estimated to be 3.7 m and 1.5 m, while the main gear strut length and diameter of a four wheel bogey are 2.8 m and 1.5 m. The relatively large nose landing gear diameter is a consequence of the leading edge camber centerbody airfoils which constrains the location and stowage of the nose landing gear. The nose gear location is set

to 0.18% of centerbody chord and results in it carrying ~20% of the aircraft weight as suggested by Raymer.[10] The slat and airfoil self-noise estimates depend on average wing chord and airframe area. The slat noise estimate uses the average chord and area of the airfoils outboard of $\eta = 0.31$ where the slats are located. The airfoil self-noise is estimated based on the average chord and the area of the entire airframe. Acoustic energy is propagated from the source to the ground using the techniques described by Evans[9] which assume spherical spreading, atmospheric attenuation within a still, uniform medium, and attenuation / amplification of acoustic energy due to incidence onto a grassy surface.

The estimation of the minimum noise for a given airframe closes the three-dimensional aerodynamic and aeroacoustic design process shown in Figure 4. If the noise and performance goals are not met, then the process is repeated using insight gained from the previous iteration. Several design iterations have thus far been conducted to achieve the current airframe and, as will be shown in the next section, the noise and performance goals appear to be attainable.

Parameter	Value
Wing area, m^2	799.3
Wing span, m	58.56
MTOW, kg	154,289
Initial Cruise L/D	23.1
Cruise Mach	0.8
Initial Cruise Altitude, ft	40,000
Outer-Wing Twist, °	-2.89
Initial Cruise Angle of Attack, °	3.69
Minimum approach velocity, m/s	64

Table 1. Geometric and aerodynamic performance parameters of the three-dimensional airframe design.

Coefficient	Value
C_L	0.2237
C_m	0.0000
C_D	0.0099
C_{Di}	0.0043
C_{Dp}	0.0007
C_{Dp} centerbody	0.0004
C_{Dp} wing	0.0003
C_{Dp} winglet	0.0000
C_{Df}	0.0043
C_{Df} centerbody	0.0032
C_{Df} wing	0.0010
C_{Df} winglet	0.0001
$C_{D, wave}$	0.0000
$C_{D,engine nacelles}$	0.0004

Table 2. Lift, moment and drag coefficients at beginning of cruise.

III.   Three-Dimensional Aerodynamic and Aeroacoustic Design Results

The iterative, quasi-inverse framework was used to create the airframe of Figure 1. The detailed design implications and strategies that have led to this design are discussed in the context of the aerodynamic and aeroacoustic performance. The focus is on the implication of these results and how an aircraft can be designed to achieve the goal of low noise emission on approach with high lift-to-drag ratio during cruise.

The key performance parameters for the aircraft together with the lift, moment, and drag coefficients at the beginning of cruise are tabulated in Tables 1 and 2. The major finding is the large lift-to-drag ratio, both in comparison to existing aircraft and to other studies of blended-wing-body type aircraft. The metric for comparison is ML/D, which is 18.5 for the aircraft design depicted in Figure 1. A modern conventional, tube-wing aircraft such as the Boeing 777 has an ML/D of 15.5.[12] Qin et al.[26] report an ML/D of 13.4 for their blended-wing-body type aircraft while Liebeck[16] attained an ML/D between 17 and 18 for a BWB of similar passenger capacity as the aircraft under study here. Diedrich et al.[6] report an ML/D of 17.5 for the SAX12 aircraft, which provided the initial two-
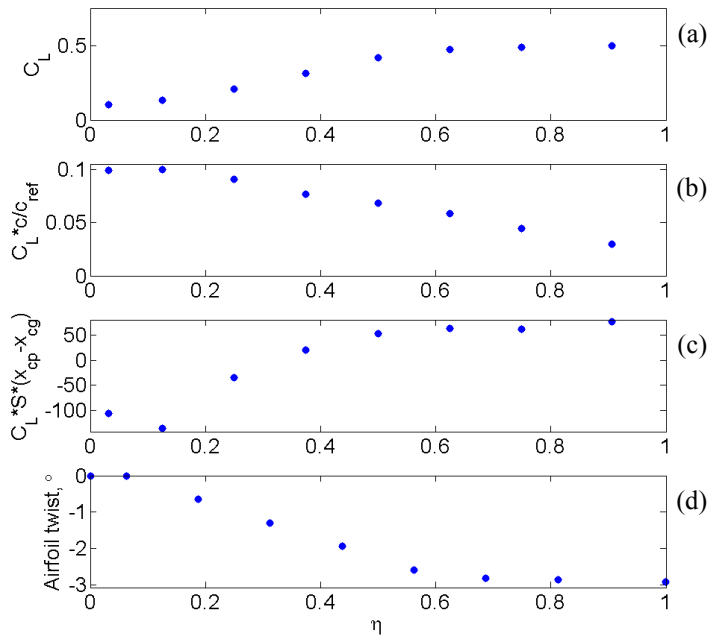
Figure 7. Sectional lift and twist distributions for the airframe as a function of spanwise location.
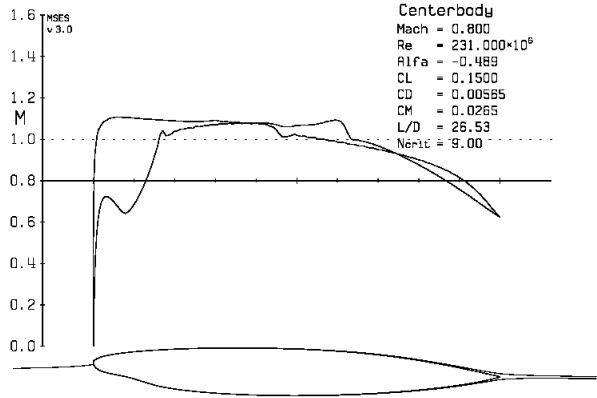
Figure 8. Two-dimensional viscous, compressible MSES analysis of the centerbody airfoil section with leading edge camber.
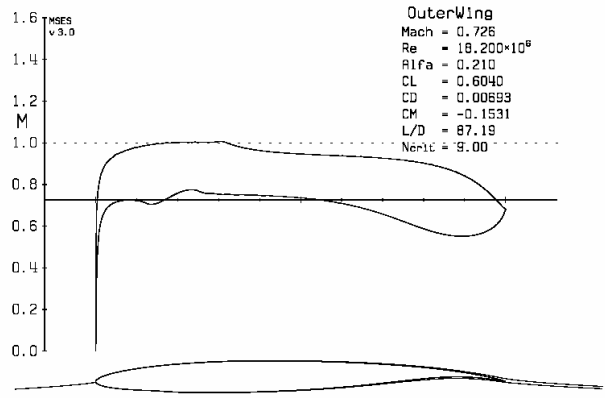
Figure 9. Two-dimensional viscous, compressible MSES analysis of the outer-wing airfoil section.

dimensional planform for this aircraft design. The resulting ML/D of 18.5 is superior in comparison to these aircraft designs. There is a small uncertainty in this result due to the Hoerner[21] estimate of centerbody drag and the assumption that wave drag is negligible, which is reasonable given the resulting Mach number distribution over the airframe. Since the analysis does not account for the drag reduction due to boundary layer ingestion into the embedded engines, a further increase in lift-to-drag ratio is expected. A separate research effort is being conduced to assess the impact of boundary layer ingestion on airframe drag. The lift and twist distributions depicted in Figure 7b and 7d reveal that the lift distribution of the airframe is largely triangular, which results in low induced drag at an acceptable angle of attack close to 3°. According to certification regulations this is the maximum cabin pitch angle allowed during cruise.

The Mach number distributions of the centerbody and outer-wing sections obtained from the two-dimensional MSES calculations are shown in Figure 8 and 9. The results indicate that the lift from the centerbody is mainly created in the forward 20% of chord while the loading of the outer wing is essentially uniformly distributed over the chord. The forward loading of the centerbody is due to the leading edge camber and, in combination with the airfoil twist and C_L distribution the moments about the aircraft center of gravity balance. Figure 7c depicts the distribution of the sectional C_L at the respective neutral points (shown as dots in Figure 5) times the moment arm. Integrating this moment distribution over the span trims the aircraft with a zero net moment. Note the pronounced effect of centerbody leading edge camber on the normalized lift and moment distributions shown in Figures 7b and 7c. Based on the large lift-to-drag ratio of the airframe, leading edge camber is considered a viable replacement for aft reflex on a blended wing body design to balance the pitching moment at the beginning of cruise. In comparison to an airframe with reflex camber, the concept of leading edge camber yields an efficient airframe with an ML/D of 18.5.
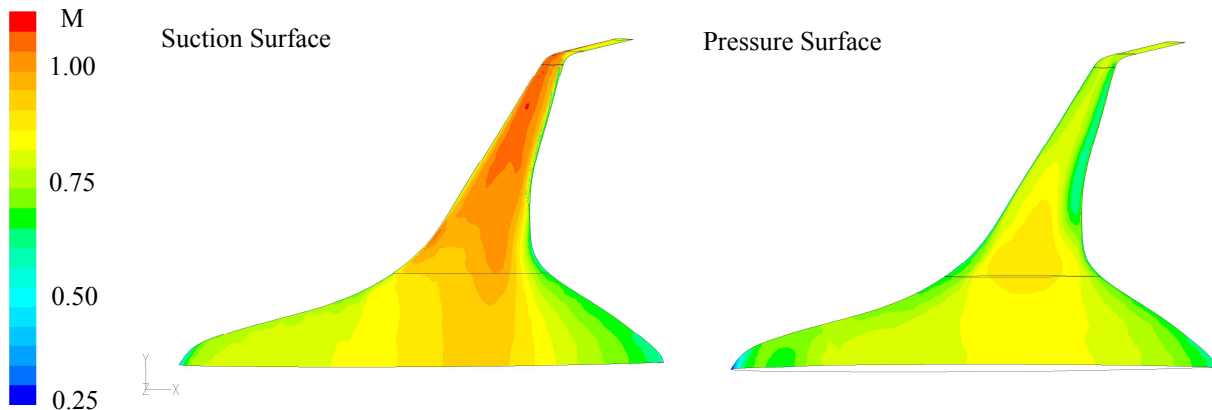

Figure 10. Three-dimensional CFD solution: Mach number contours on suction and pressure surface of the airframe.
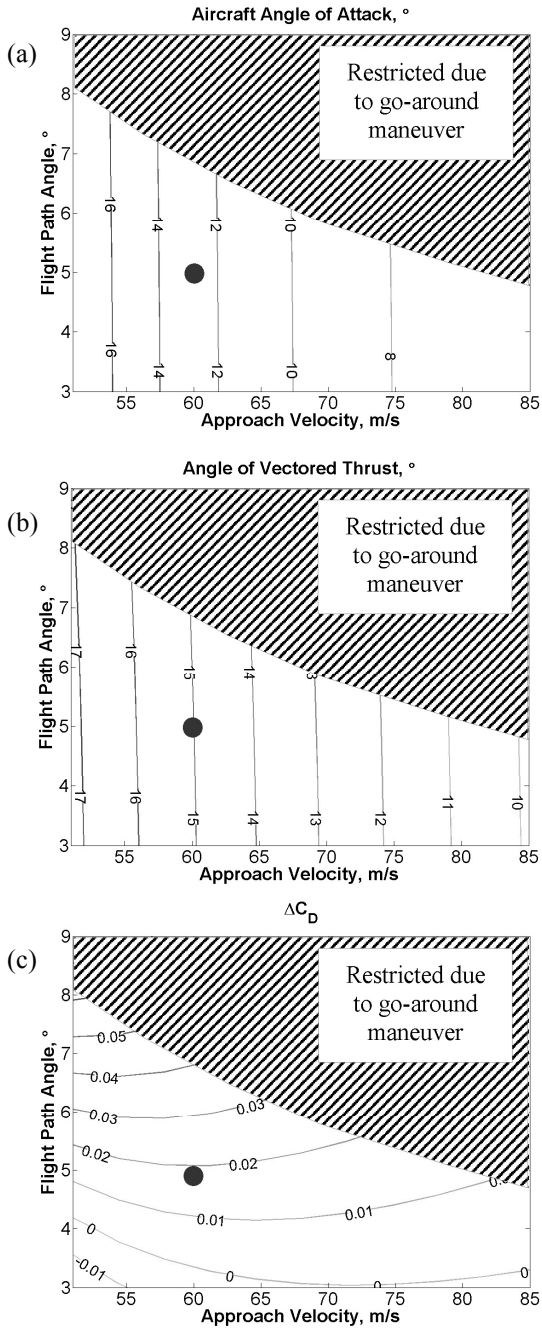
Figure 11. Approach trajectory variation in (a) aircraft angle of attack, (b) vectored thrust angle, and (c) required increase in drag. Solid circle indicates design point.
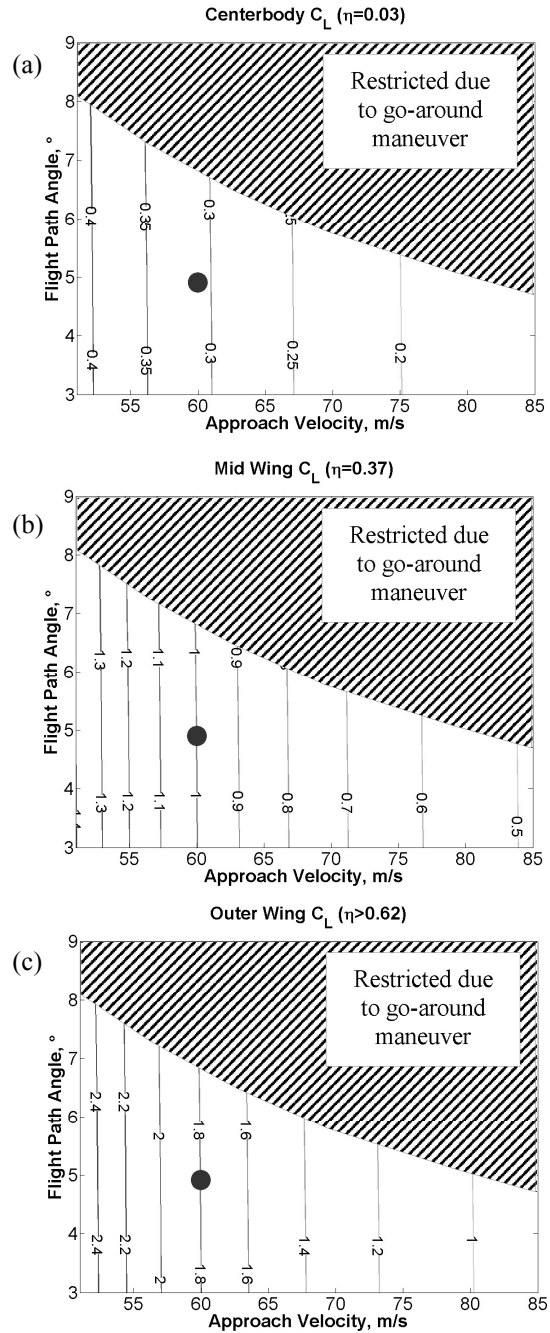
Figure 12. Approach trajectory variation in lift coefficient for (a) centerbody, (b) mid-wing, and (c) outer-wing. Solid circle indicates design point.

This is due to a low induced drag and wave drag without penalties in trim drag.

The three-dimensional Euler calculations are shown in Figure 10. The results, reveal an essentially shock free flow field with the majority of the airframe experiencing Mach numbers below 1.15. The exception to this is a small region on the lower portion of the winglet, which has negligible impact on the overall flow field and can be eliminated through careful redesign of the winglet. Since strong shocks are absent, the wave drag of the three-dimensional airframe is assumed to be negligible. Comparing the two-dimensional calculation of the centerbody in

Figure 8 with the three-dimensional Euler solution in Figure 10, where the former indicates a weak shock and the latter a fully subsonic Mach number distribution on the centerbody, shows the necessity of a full three-dimensional assessment and the need to capture the effects of three-dimensional relief.

The approach performance analysis was conducted for a range of approach velocities and flight path angles. The results are shown in Figure 11a and 11b where the thrust vectoring angle is comparable to the angle of attack for all approach profiles considered, essentially aligning the vectoring of the jet exhaust with the free-stream direction. This yields a minimal amount of cross-flow experienced by the jet exhaust and, in combination with the relatively low exhaust velocities, suggests a reduction in exhaust noise during approach. In comparison to other trim devices such as elevators, which result in the creation of noise when deflected, thrust vectoring is suggested to be an

Figure 13. Drag polars of centerbody, mid-wing, and outer-wing airfoils at M=0.176 (60 m/s); based on two-dimensional analysis.

effective and quiet means to trim the pitching moment during approach. Figure 11c depicts the required amount of additional drag to keep the aircraft on the glide slope. For the target approach profile of 60 m/s and 5°, a ΔC_D of 0.02 is required and research is currently being conducted on deployable drag devices and engine air brakes to dissipate the corresponding amount of energy quietly.

The required sectional lift coefficients for the centerbody, mid-wing and outer-wing sections are shown in Figure 12. The desired low noise approach path is marked by solid circle. These are three-dimensional lift coefficients that were converted from two-dimensional values by $C_{L,3D} = C_{L,2D}/\cos^2\Lambda$.[21] In order to fly an approach velocity less than 60 m/s with the current airframe, the three main airfoil sections must create lift coefficients greater than 0.3, 1.0, and 1.8, respectively. It is difficult to achieve lift coefficients far exceeding 1.8 with a fixed geometry, 7% thick airfoil while meeting FAR 25.125 requirements and low wave drag at cruise. Therefore, high-lift capability is essential to a low noise airframe design and enables a slow and steep approach profile. The implementation and assessment of quiet high-lift devices are currently being investigated in separate research.

The drag polar data obtained from an MSES analysis at a flight Mach number of 0.176 for the centerbody and mid- and outer-wing sections are given in Figure 13. The results can be directly compared to the required C_L data of Figure 12. The lift requirements for a quiet approach path are within the aerodynamic capability of the centerbody and mid-wing airfoils, but are slightly beyond that of the outer-wing. With an outer-wing C_{Lmax} of 1.58, an approach speed of 64 m/s is possible with a resultant OASPL of approximately 65 dBA. With an unconventional high-lift device such as for example leading edge rotating cylinders or leading edge boundary layer suction, the current airfoil might also achieve the 60 m/s approach speed necessary for a quiet landing. Thus, the preliminary airframe design presented in this paper yields a highly-efficient airframe, but it does not yet meet the aggressive noise goals of the Silent Aircraft Initiative.

IV.   Conclusions and Outlook on Achieving the Goal of a Silent Aircraft

A suite of high and low fidelity aircraft design tools have been combined with operational and aero-acoustic considerations to create a new design methodology for the detailed three-dimensional design of a blended-wing-body type aircraft with quiet approach capability and advanced cruise lift-to-drag ratios. The aircraft design incorporates centerbody leading edge camber to balance the pitching moment during cruise eliminating the need for reflex cambered airfoils, which can compromise cruise performance. Thrust vectoring, quiet drag augmentation, and leading edge high-lift are considered to balance the forces acting on the aircraft during approach. The presented, preliminary blended-wing-body type airframe design is highly efficient with an ML/D of 18.5, but it does not yet fully meet the aggressive noise reduction goal set out by the Silent Aircraft Initiative due to limitations on the low speed, high-lift performance of the fixed geometry outer-wing. To reach the noise goal, the planform and airfoils comprising the three-dimensional aircraft geometry need to be modified according to the design philosophy described in Figure 3. The idea is to further reduce the approach velocity by increasing the maximum attainable lift
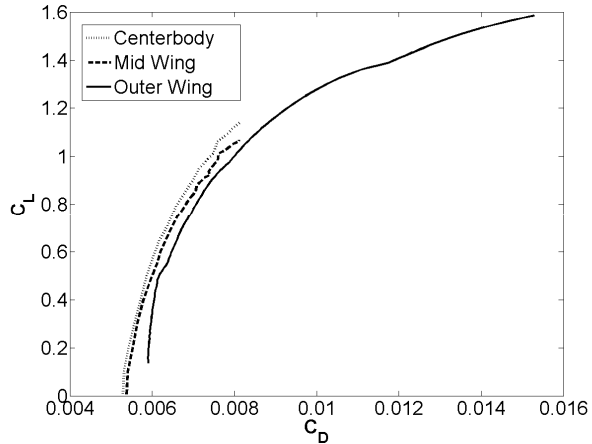
coefficient on the outer-wing while also increasing the outer wing area to lower the lift coefficient required for a low approach velocity. The lowered approach velocity comes at the expense of a penalty in cruise drag coefficient and structural weight. A preliminary MSES analysis has shown that modification to the nose of the existing airfoil might result in a C_{Lmax} that could yield the 60 m/s quiet approach speed; thus, the outer-wings of the current airframe will be optimized to increase C_{Lmax} with minimal increase in cruise drag. A preliminary AVL analysis was conducted on an airframe with total area of 850 m^2 where the area increase came from the outer-wings as shown in Figure 3. The required lift coefficient on the outer-wing dropped to 1.3, but the cruise ML/D decreased to roughly 17.

Future work will be conducted to achieve the goal of low noise and advanced cruise performance through:

- A redesign of the outer-wing sections for lower approach velocities by increasing the maximum C_L at low speed,

- An increase in outer-wing area to lower the approach velocity for a given outer-wing C_L,

- An assessment of quiet leading edge high-lift devices to determine the maximum increase in low speed C_L without a significant noise penalty. The stall speed requirement will be used with this maximum C_L to yield an improved estimate of the minimum approach speed and resulting noise emission.

Based on the airframe design described in this paper and the proposed future tasks, it is hypothesized that an airframe can be designed which meets the noise goal of the Silent Aircraft Initiative while achieving fuel efficiency comparable to modern commercial aircraft.

Acknowledgments

References

[1] Manneville, A., Pilczer, D., and Spakovszky, Z., "Noise Reduction Assessments and Preliminary Design Implications for a Functionally-Silent Aircraft," AIAA Paper 2004-2925, 2004.

[2] Hall, C. A. and Crichton, D., "Engine and Installation Configurations for a Silent Aircraft," ISABE-2005-1164, 2005.

[3] Hall, C. A. and Crichton, D., "Engine Design Studies for a Silent Aircraft," GT2006-90559, to be presented at the ASME Turbo Expo, Barcelona, May 2006.

[4] Agarwal, A. and Dowling, A. P., "Low Frequency Acoustic Shielding of Engine Noise by the Silent Aircraft Airframe," AIAA 2005-2996, 2005.

[5] Crichton, D., Xu, L., and Hall, C. A., "Preliminary fan design for a Silent Aircraft," GT2006-90564, to be presented at the ASME Turbo Expo, Barcelona, May 2006.

[6] Diedrich, A., Hileman, J., Tan, D., Willcox, K., Spakovszky, Z. "Multidisciplinary Design and Optimization of the Silent Aircraft," AIAA Paper 2006-1323, 2006.

[7] Fink, M.R., *Airframe Noise Prediction Method*. FAA-RD-77-29, 1977 (available from DTIC as AD A039 664).

[8] Chinoy, C.B., "Airframe Noise Prediction," *Engineering Sciences Data Unit (ESDU) Airframe Noise Prediction Manual*, Item No. 90023 Amendment C, ESDU International plc, London, UK, June 2003.

[9] Evans, P., "An Introduction to Aircraft Noise Lateral Attenuation," *Engineering Sciences Data Unit (ESDU) Lateral Attenuation Manual*, Item 81035, ESDU International plc, London, UK, Nov. 1981.

[10] Raymer, D.P., Aircraft Design: A Conceptual Approach. Third Edition, American Institute of Aeronautics and Astronautics, Inc., Reston VA, 1999.

[11] Jaeger, S.M., Burnside, N.J., Soderman, P.T., Horne, W.C., and James, K.D., "Microphone Array Assessment of an Isolated 26%-Scale, High-Fidelity Landing Gear," AIAA Paper 2002-2410, 2002.

[12] Lee, J.J., Lukachko, S.P., Waitz, I.A. and Schafer, A., "Historical and Future Trends in Aircraft Performance, Cost and Emissions," *Annu. Rev. Energy Environ.*, Vol. 26, pp. 167–200, 2001.

[13] Sakaliyski, K.D., Aeroacoustics of Perforated Drag Plates for Quiet Transport Aircraft, S.M. thesis, Massachusetts Institute of Technology, 2005.

[14] Manneville A., Propulsion System Concepts for Silent Aircraft. S.M. thesis, Massachusetts Institute of Technology, 2004.

[15] Wakayama, S., "Blended-wing-body optimization problem setup" AIAA Paper 2000-4740, 2000.

[16] Liebeck, R.L., "Design of the Blended-Wing-Body Subsonic Transport," *Journal of Aircraft*, Vol. 41, No. 1, pp. 10-25, 2004.

[17] Drela, M. and Youngren, H., "AVL Summary," http://raphael.mit.edu/avl/, 12 Nov 2005.

[18] Drela, M. and Giles, M.B., "Viscous-Inviscid Analysis of Transonic and Low Reynolds Number Airfoils," *AIAA Journal*, Vol. 25, No. 10, pp. 1347-1355, 1987.

[19] Drela, M., "Design and Optimization Method for Multielement Airfoils," AIAA Paper 93-0960, 1993.

[20] Drela, M., "A User's Guide to MSES 3.0," March 2004.

[21] Hoerner, S.F., Fluid Dynamic Drag. Published by the author, 1965.

[22] Shevell, R. S., Fundamentals of Flight. Second Edition, Prentice Hall, Inc., 1989.

[23] Reynolds, T.G. and Clarke, J-P., "Operational Considerations for Silent Aircraft Design," Version 2.0, *Silent Aircraft Initiative Internal Document*, May 7, 2004.

[24] Shank, E. M. and Hollister, K. M., "Precision Runway Monitor", *MIT Lincoln Laboratory Journal*, Vol. 7, No. 2, pp. 329-353, 1994.

[25] Midkiff, Capt. Alan H. (American Airlines), Personal communication, May 20, 2004.

[26] Qin, N., Vavalle, A., Le Moigne, A., Laban, M., Hackett, K., and Weinerfelt, P., "Aerodynamic Considerations of Blended-Wing-Body Aircraft," *Prog. Aero. Sciences*, Vol. 40, pp. 321-343, 2004.